rat MSCs has been described previously [25]. Nuclei were counterstained with DAPI. Positive fluorescence signals appeared as multiple dots in the nucleus. Green and yellow indicated rat and mouse chromosomes, respectively. For simultaneous analysis of immunofluorescence and FISH on the same sections, immunofluorescence was performed prior to FISH to avoid attenuation of antigenicity.

### Chemotaxis assays

We used recombinant human chemokine (C-X-C motif) ligand 12 (CXCL12)/stromal derived factor-1α [SDF-1α (PeproTech Inc., Rocky Hill, NJ, USA)], VEGF (Abnova, Taipei, Taiwan), platelet-derived growth factor BB (PDGF-BB), or IL-6 (PeproTech) as chemoattractants. For MSC migration assays, $3 \times 10^5$ eGFP-labeled MSCs were seeded in the upper well of a 24-well Transwell Boyden chamber (polycarbonate membranes, 8.0-μm pore size; Corning, Lowell, MA, USA) and allowed to migrate toward the bottom well containing serum-free medium with 100 ng/mL of the indicated chemoattractants for 24 h. Migrating cells were counted under a BZ-9000 BIOREVO all-in-one fluorescence microscope (Keyence, Osaka, Japan).

### Microarray analysis

RNA was extracted from xenografts of COLO 320 cells alone or COLO 320 cells co-implanted with rat MSCs from NOG mice using an RNeasy kit and analyzed with a Human Oligo chip 25 K 3D-Gene (Toray, Tokyo, Japan).

Transcript Profiling: Accession No: GSE29389.

### Cell transduction

To generate stable VEGF over-expressing (VEGF OE) and CXCL12 knockdown (CXCL12 KD) cell lines, COLO 320 cells were transduced with lentiviruses for VEGF or CXCL12 shRNA expression (GenTarget, San Diego, CA, USA) for 72 h according to the manufacturer's instructions. These stable cell lines were subjected to the xenograft analysis in SCID mice as described previously. The total number of mice used in this experiment was 15.

### Co-culture of human colon cancer cell lines with rat MSCs

To examine heterotypic interactions between colon cancer cells and MSCs, MSCs were co-cultured with COLO 320 and HT-29 colon cancer cells either directly or indirectly using a Transwell culture dish. Moreover, monocultured colon cancer cells were treated with MSC-conditioned medium (MSC-CM) or recombinant human CXCL12. Co-cultured COLO 320 cells were also treated with neutralizing antibodies against human E-cadherin (Takara, Otsu, Japan), CCL5 (R&D Systems Inc., Minneapolis, MN, USA), or CD49d (α4 integrin, Pierce Biotechnology, Rockford, IL, USA) (Supplementary Table 2), or a small molecule antagonist of CXCR4, AMD3100 (Sigma-Aldrich, Saint Louis, MO, USA), or an γ-secretase inhibitor [(3,5-difluorophenylacetyl)-Ala-Phg-OBu, DAPT, PEPTIDE, Minoh, Japan].

### Cell cycle analysis and apoptosis

Cell cycle distribution was analyzed by flow cytometry and Ki-67 immunohistochemistry (Abcam, Cambridge, MA, USA) (Supplementary Table 2). Ki-67 immunohistochemistry was performed according to the manufacturer's instructions. Apoptosis was measured by terminal deoxynucleotidyl transferase-mediated dUTP nick-end labeling (TUNEL) reactions using the DeadEnd Colorimetric TUNEL system (Promega, Madison, WI, USA).

### Western blot analysis of AKT, mitogen-activated protein kinases (MAPKs), and EMT signaling molecules

Each cell population separated by FACS was lysed in radioimmunoprecipitation assay buffer comprising 20 mM Tris–HCl (pH 7.4), 150 mM sodium chloride, 1 mM EDTA (pH 8.0), 0.1 % (w/v) SDS, 0.1 % sodium deoxycholate, 1 % Triton X-100, and one tablet each of complete Mini protease inhibitor cocktail and PhosSTOP phosphatase inhibitor cocktail tablets (Roche Diagnostics, Mannheim, Germany). Forty micrograms of each lysate, as determined by a Bio-Rad protein assay (Bio-Rad, Hercules, CA, USA), were resolved on a 12 % denaturing polyacrylamide gel and transferred to a polyvinylidene difluoride membrane. After blocking with 5 % nonfat dry milk in TBS, the membrane was incubated with primary antibodies against pan-AKT phospho-AKT (Ser473), JNK1/3, phospho-SAPK/JNK, p38, phospho-p38, SNAIL, E-cadherin, vimentin, or β-actin (Supplementary Table 2), followed by a horseradish peroxidase-conjugated secondary antibody (Santa Cruz Biotechnology, Santa Cruz, CA, USA). Immunoreactions were developed using an enhanced chemiluminescence kit (Amersham Biosciences, Little Chalfont, England).

### Cell proliferation assay

COLO 320 cell proliferation was directly measured by flow cytometry. Briefly, co-cultured MSCs with or without neutralizing antibodies against human E-cadherin, CCL5, CD49d (α4 integrin), or γ-secretase inhibitor (DAPT), and

a small-molecule antagonist of CXCR4, AMD3100 were eliminated by gating GFP, and the viable single COLO 320 cell number was counted at 24, 48, and 72 h co-cultivation. These data were compared with the control of co-cultured COLO 320 without any treatments (Fig. 5c).

### Statistical analysis

To compare two groups, parametric and nonparametric analyses were performed using the unpaired Student's *t* test and the Mann–Whitney *U* test, respectively. Categorical variables were compared using the Chi square test, the exact *P* value based on Pearson's statistic, or the Monte Carlo method. For multiple comparisons in in vivo studies, we employed analysis of variance (ANOVA), particularly in serial assessments, and two-way repeated measurements (mixed between or within subjects) ANOVA followed by Bonferroni's test. A difference was considered significant when $P$ was $< 0.05$ in all two-tailed tests. Measured values obtained from the study are presented as mean ± standard error of means unless otherwise indicated. SPSS Statistics 17.0 software (SPSS Inc., Chicago, IL, USA) was used for all statistical analyses.

## Results

### MSC dependency for xenograft tumor progression

Xenografted tumor growth appeared to occur as two categories according to their dependency or lack of dependency on co-implanted MSCs. DLD-1, HCT-15, and HT-29 cells were MSC-independent, whereas COLO 320, HCT116, and LoVo cells were MSC-dependent in SCID mice (horizontal panels in Fig. 1a). We chose the two most distinctive cell lines, COLO 320 as an MSC-dependent cell line and HT-29 as an MSC-independent cell line, for subsequent analyses. To differentiate the effects of tumor immune surveillance from the net effects of MSCs on tumor progression, we examined three classes of immunodeficient mice as recipients of xenografts, namely nude mice, which have impaired T cell functions, SCID mice with impaired T cell and B cell functions, and NOG mice. Compared with the NOD strain, NOG mice have decreased NK and macrophage activities, and are defective for T and B cell functions from the scid mutation and exhibit dendritic cell dysfunction from an IL-2Rγ mutation [18]. NOG mice show very limited transplantation rejection. Therefore, they are an excellent model for human xenograft studies. In nude mice (bottom panels in Fig. 1a), engraftment of xenografts was delayed for both MSC-dependent and -independent cell lines, resulting in a smaller maximum tumor volume than that in SCID and NOG mice on day 13. Furthermore, COLO 320 xenografts without MSCs were successfully engrafted into NOG mice at approximately 2 weeks after implantation (top right panel in Fig. 1a).

### Angiogenic profiles of xenograft tumors

Measurement of angiogenesis is complicated by the fact that it is a dynamic process, although most studies to date have focused on the products of angiogenesis such as VEGF family proteins [26] and MVD, which are common endpoints for assessment of tumor vascularity [23]. Therefore, we evaluated the angiogenic profiles by the expression of VEGF and other angiogenic proteins, including HGF and FGF-2, as well as MVD. VEGF mRNA expression was significantly higher in HT-29 xenografts than in COLO 320 xenografts, while there was no difference between either xenograft with and without MSCs (Fig. 1b). VEGF protein expression was significantly higher in HT-29 cells (3.35 ± 0.15 ng/mL) than that in COLO 320 cells (1.26 ± 0.47 ng/mL, $P = 1.65\text{E}{-4}$), while HGF and FGF-2 proteins were produced at the same level in the two cell lines (Supplementary Fig. 1c, d). Although cancer cell nests were sparser, the surrounding tumor stroma with tumor microvessels was more abundant in COLO 320 + MSC xenografts than in HT-29 + MSC xenografts (Fig. 1c). 'Modified MVD' was significantly greater in COLO 320 xenografts (1.60 ± 0.07 $mm^{-2}$) than in HT-29 xenografts (0.87 ± 0.03 $mm^{-2}$, $P = 0.0026$; Fig. 1d). The number of MSC-derived (eGFP-positive) cells progressively increased as COLO 320 xenografts advanced, particularly at 15 mm in diameter, while the number of these cells was low in HT-29 xenografts regardless of tumor size (Fig. 1e). Although MSCs successfully engrafted, rat *Vegf* was not detected by qRT-PCR, suggesting that rat Vegf produced by engrafted MSCs was less likely to directly compensate for human VEGF in co-implanted COLO 320 xenografts (Fig. 1f). Consequently, these results suggest that angiogenesis in COLO 320 xenografts occurs less depending on VEGF than HT-29 xenografts.

### Fate of co-implanted eGFP-labeled rat MSCs in xenograft tumors

Engrafted MSCs were randomly distributed in the COLO 320 xenograft tumor stroma, potentially as CAFs, as previously reported (data not shown). Excluding CAFs, MSC-derived cells were primarily located in perivascular regions on day 14 after implantation (Fig. 2a). Several differentiation markers for pericytes, including Thy-1 (CD90; Fig. 2b), NG2 (Fig. 2c), and αSMA (Fig. 2d), largely or partially co-localized with eGFP, while platelet endothelial

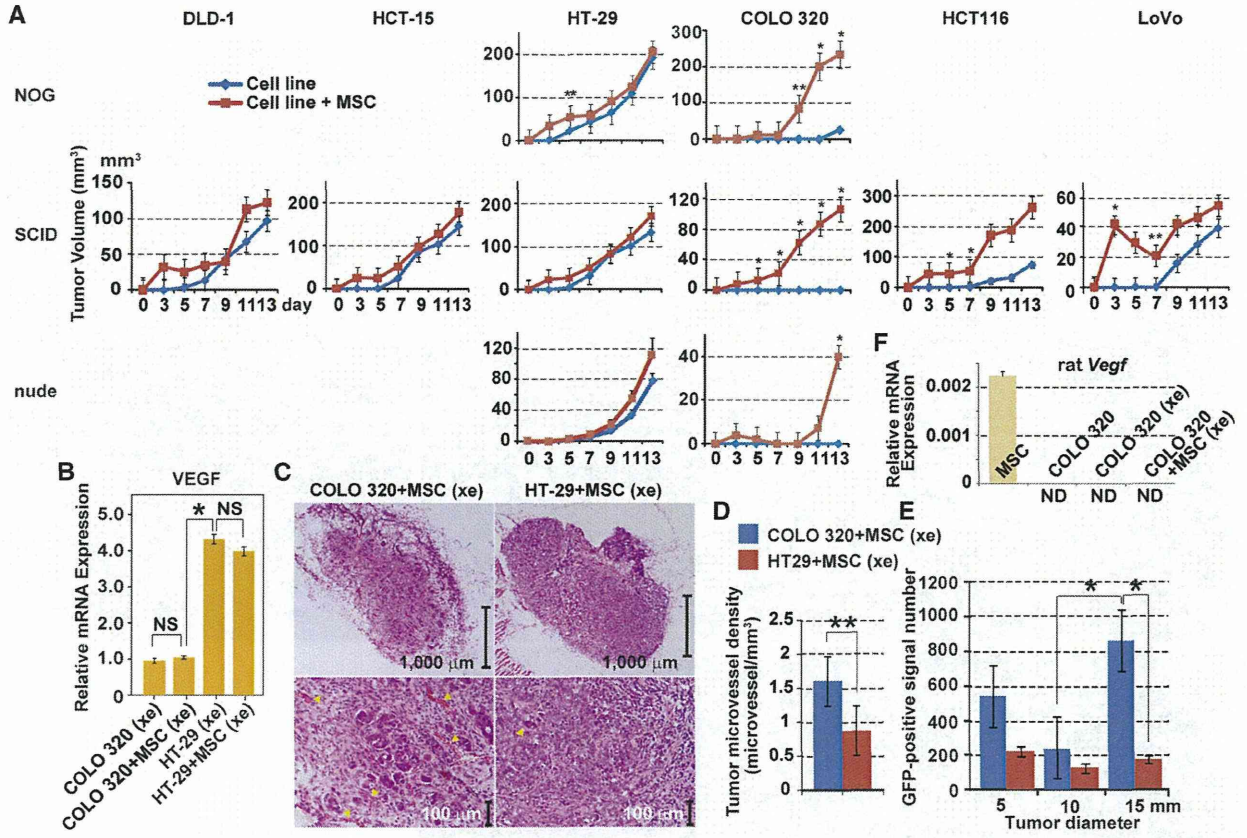


**Fig. 1** Growth dependency and angiogenic profiles of MSC-co-implanted xenografts. **a** The tumor volume of xenografts established using six human colorectal cancer lines with or without co-implanted rat MSCs in the three class of immunodeficient mice was measured over 2 weeks. *Horizontal panels* designated as SCID show the dependency of tumor growth on co-implanted MSCs in all the six cell lines. MSC-independent cell lines were DLD-1, HCT-15, and HT-29 in SCID mice (*left half*), whereas MSC-dependent cell lines were COLO-320, HCT-116, and LoVo (*right half*). *Two rows of vertical panels* indicate HT-29 (*left*) and COLO-320 (*right*) xenograft analyses in the three class of immunodeficient mice. **b** VEGF transcripts were analyzed by qRT-PCR in xenografted tumors. **c** H&E-stained COLO-320 and HT-29 xenografts with co-implanted MSCs at low magnification (*upper panels*) and high magnification (*lower panels*). *Yellow arrowheads in the lower panels* indicate tumor vessels. **d** The modified MVD was estimated as the mean MVD of triplicates from COLO-320 and HT-29 cells. **e** Comparison of the number of GFP-positive signals obtained from tumors grown up to 5, 10, or 15 mm in diameter. The number of GFP-positive signals are expressed as mean ± SEM in three representative sections, respectively. **f** Relative rat-specific *Vegf* mRNA expression was compared in MSCs, COLO-320 cells, and COLO-320 xenografts with/without MSCs. *NS* and *ND* indicate 'not significant' and 'not detectable', respectively. *Asterisks* indicate statistical significance: $*P \leq 0.05$, $**P \leq 0.01$, $***P \leq 0.001$. **a** $P = 0.0048$ on day 5 of HT-29 xenografts in NOG mice; $P = 0.003$, 0.047, and 0.014 on days 9, 11, and 13 of COLO 320 xenografts in NOG mice; $P = 0.020$, 0.021, 0.013, 0.039, and 0.022 on days 5, 7, 9, 11, and 13 of COLO 320 xenografts in SCID mice; $P = 0.036$ on day 13 of COLO 320 xenografts in nude mice; $P = 0.017$ on day 5 and $P = 0.03$ on day 7 in the HCT-116 panel; $P = 0.025$ on day 3 and $P = 0.004$ on day 7 in the LoVo panel. **b** $P = 0.0048$ on day 5 of HT-29 xenografts in NOG mice. **e** $P = 0.043$ between 10 and 15 mm in the COLO 320 xenograft and $P = 0.031$ between COLO 320 and Ht-29 xenograft in 15 mm tumor diameter

cell adhesion molecule-1 (PECAM-1, CD31), a representative endothelial marker, did not co-localize, but was in close contact with eGFP-positive cells at the perivascular niche (Fig. 2e, f). These observations suggest that MSCs repopulate at the perivascular niche and differentiate into pericytes in COLO 320 xenograft tumors.

In contrast to COLO 320 xenografts, most MSCs were likely to engraft randomly as CAFs in the HT-29 xenograft tumor stroma (Fig. 2g), which partially expressed the representative myofibroblast marker, αSMA (Fig. 2h–k). Perivascular MSCs were seldom observed in HT-29 xenografts (Fig. 2l), while they were abundantly observed in COLO 320 xenografts.

## Characterization of recruited mouse cells adjacent to rat MSC-derived cells

Rat MSCs were in line with or immediately adjacent to mouse cells (Fig. 3a, b). In simultaneous immunofluorescence analyses, mouse-derived cells recruited to the tumor

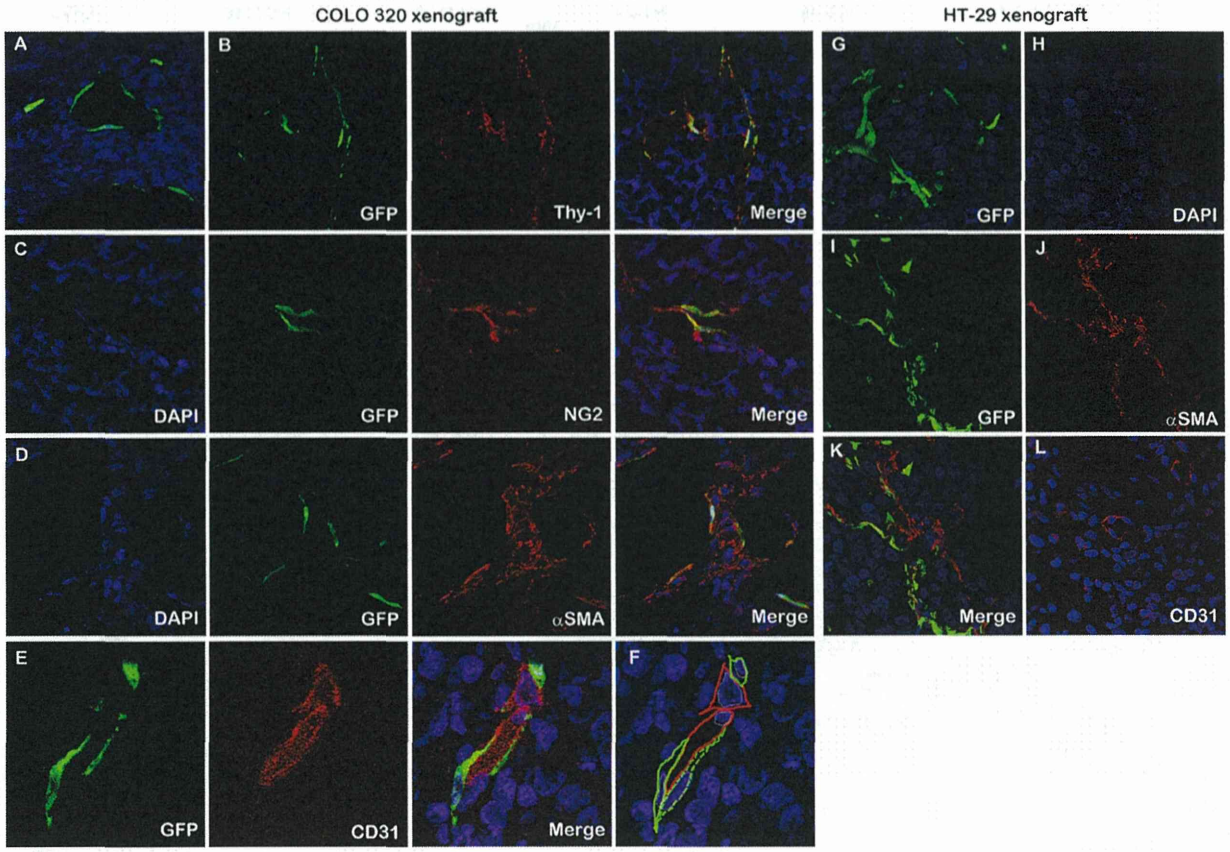


**Fig. 2** Fate of GFP-positive MSC-derived cells in COLO-320 and HT-29 xenografts. **a** MSC-derived cells producing GFP fluorescence-populated areas along the inner vascular lumen in the COLO 320 tumor stroma. Cells were counterstained with DAPI. Pericyte markers, including Thy-1 (CD90) (**b**), NG2 chondroitin sulfate proteoglycan (**c**), and αSMA (**d**) were stained with Alexa Fluor 594-labeled antibodies in the COLO 320 tumor stroma. **f** Is a schematic representation of **e**. **g** MSC-derived cells producing GFP fluorescence randomly populated the HT-29 tumor stroma. **h** Cells were counterstained with DAPI. **j** αSMA was stained with an Alexa Fluor 594-labeled antibody. **k** Merged image of **h–j**. **l** Representative immunofluorescence of CD31 in the HT-29 tumor stroma

vessels differentiated mainly into CD31-positive endothelial cells (Fig. 3c), while some differentiated into αSMA-positive mural cells (Fig. 3d). These findings were more frequently observed in COLO 320 + MSC xenografts than in HT-29 + MSC xenografts (data not shown), which may explain why MVD was significantly greater in COLO 320 xenografts than in HT-29 xenografts, suggesting that rat MSC-derived cells recruited mouse angiogenic cells at possible sites of tumor vasculogenesis in COLO 320 xenografts. Whether these mouse cells are truly angiogenic cells or recruited at the site of tumor vasculogenesis should be warrant by further analysis.

## Selective activation of the CXCL12/CXCR4 axis in COLO 320 xenografts co-implanted with MSCs

To investigate chemoattractants of rat MSCs, we evaluated ligand–receptor interactions for CXCL12/Cxcr4 [27], VEGF/Vegfr1(Flt1), Vegfr2 (Kdr) [26] PDGF-BB/Pdgfr-β [28], and IL-6/Il-6r α chain [29], all of which have been previously reported to act as MSC chemoattractants (Fig. 4a, b). Among these factors, human CXCL12 was unique and the most potent chemotactic factor to Cxcr4-bearing rat MSCs (Fig. 4c–f). qRT-PCR analysis revealed that *CXCL12* was the most upregulated gene among 58 upregulated genes of the 25,000 genes examined by microarray comparing co-implanted COLO 320 xenografts with COLO 320 xenografts alone (Fig. 4g, h). CXCL12 was expressed at baseline in COLO 320 cells and was not influenced by co-culture with MSCs; however, it was slightly upregulated in xenografts and dramatically upregulated in co-implanted xenografts, consistent with the transcriptomic data obtained from the microarray analysis. In contrast, HT-29 cells failed to express *CXCL12* under any of the conditions. *CXCR4* was slightly upregulated in co-cultured COLO 320 cells and markedly upregulated in

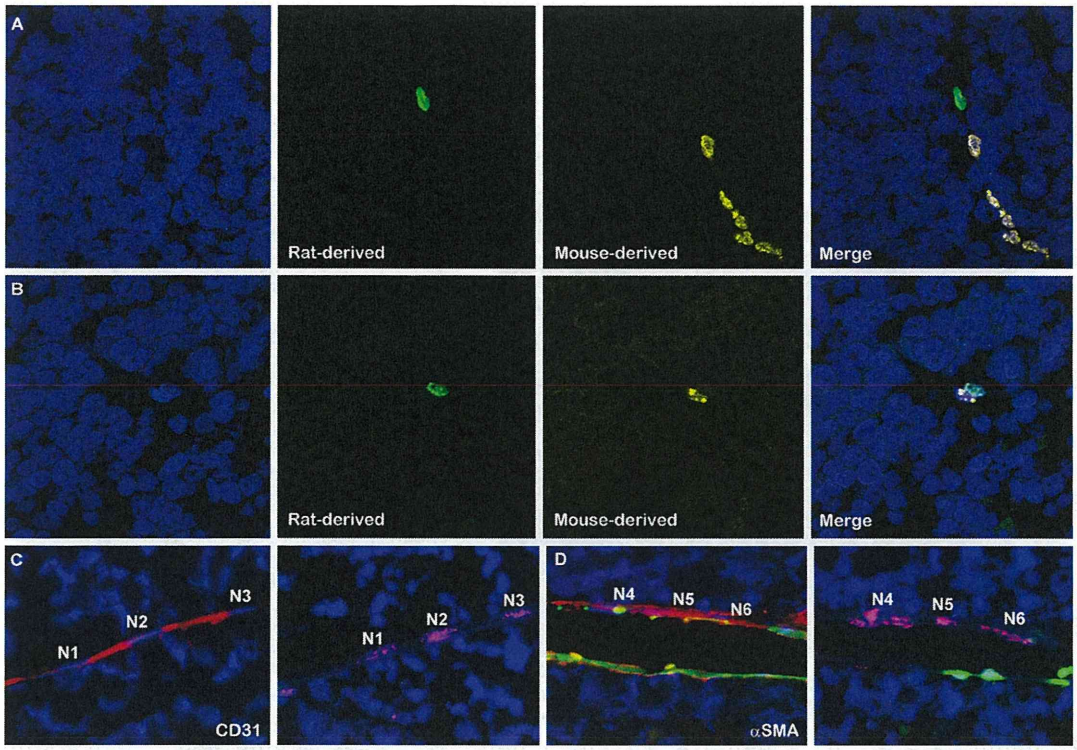


**Fig. 3** Characterization of recruited mouse cells located adjacent to rat MSC-derived cells in COLO-320 xenografts. Using species-specific probes, we easily differentiated human, rat, and mouse cells in xenograft tumors by two-color FISH analysis (**a**, **b**) and simultaneous immunofluorescence analyses of CD31 (**c**) and αSMA (**d**) on the same sections analyzed by FISH. N1–6 in **c** and **d** indicate corresponding nuclei. MSC-derived cells produced green fluorescence from SpectrumGreen-labeled DNA probes while mouse angiogenic cells exhibited yellow fluorescence from Cy3-labeled DNA probes. Nuclei were counterstained with DAPI. *Pink signals in nuclei* indicate positive signals in FISH using the mouse-specific probe, while *red signals* in the cytoplasm indicate positive signals for CD31 (**c**) and αSMA (**d**) using immunofluorescence

xenografts with or without MSCs, whereas *CXCR4* was expressed at a low level in HT-29 cells under all conditions (Fig. 4i). Although analogous to rat *Vegf* (Fig. 1f), rat Cxcl12 produced by engrafted MSCs was less likely to directly compensate for tumor CXCL12 (Fig. 4j). However, in contrast to *Vegf*, rat MSCs significantly induced human *CXCL12* expression in xenograft tumors (Fig. 4i, $P = 0.017$).

To explore what attributes MSC-dependency to COLO 320 cells, we established CXCL12 knockdown (CXCL12 KD) and VEGF-overexpressing (VEGF OE) COLO 320 cells and initiated xenograft tumors using these stable lines. Xenograft tumor growth from the CXCL12 KD line was significantly inhibited; in contrast, tumor growth from the VEGF OE line was enhanced compared to that from mock transfectant. Either transgenic or knockdown cells as well as parental COLO 320 cells could not develop xenograft tumors without MSC co-implantation (Fig. 4k). These results suggested that tumor CXCL12 attributed MSC-dependent tumor growth to COLO 320 whereas tumor VEGF could not contribute to MSC-independent growth.

## Interactions between rat MSCs and human colon cancer cell lines

Co-cultured MSCs significantly increased the Ki-67 labeling index of COLO 320 cells both at 48 h ($P = 0.044$) and 72 h ($P = 0.004$), while there was an increased apoptotic index of HT-29 cells at both 48 h ($P = 0.002$) and 72 h ($P = 0.006$, Fig. 5a). These data supported by cell cycle analysis (Supplementary Fig. 1d, e) suggest that MSCs as the cancer niche affected the proliferation of these tumor cell lines in quite different ways, with a protumorigenic effect on COLO 320 cells but an anti-tumorigenic effect on HT-29 cells. In COLO 320 cells, AKT protein was exclusively activated, or phosphorylated (Fig. 5b). This effect did not occur with indirect co-culture, MSC-CM, or recombinant CXCL12 treatment, but instead AKT was activated in the direct co-culture via a cell–cell contact-dependent mechanism with MSCs, namely, via a cancer niche. In sharp contrast to COLO 320 cells, MSCs suppressed AKT signaling but clearly activated or phosphorylated p38 in the co-cultured HT-29 cells in the cancer

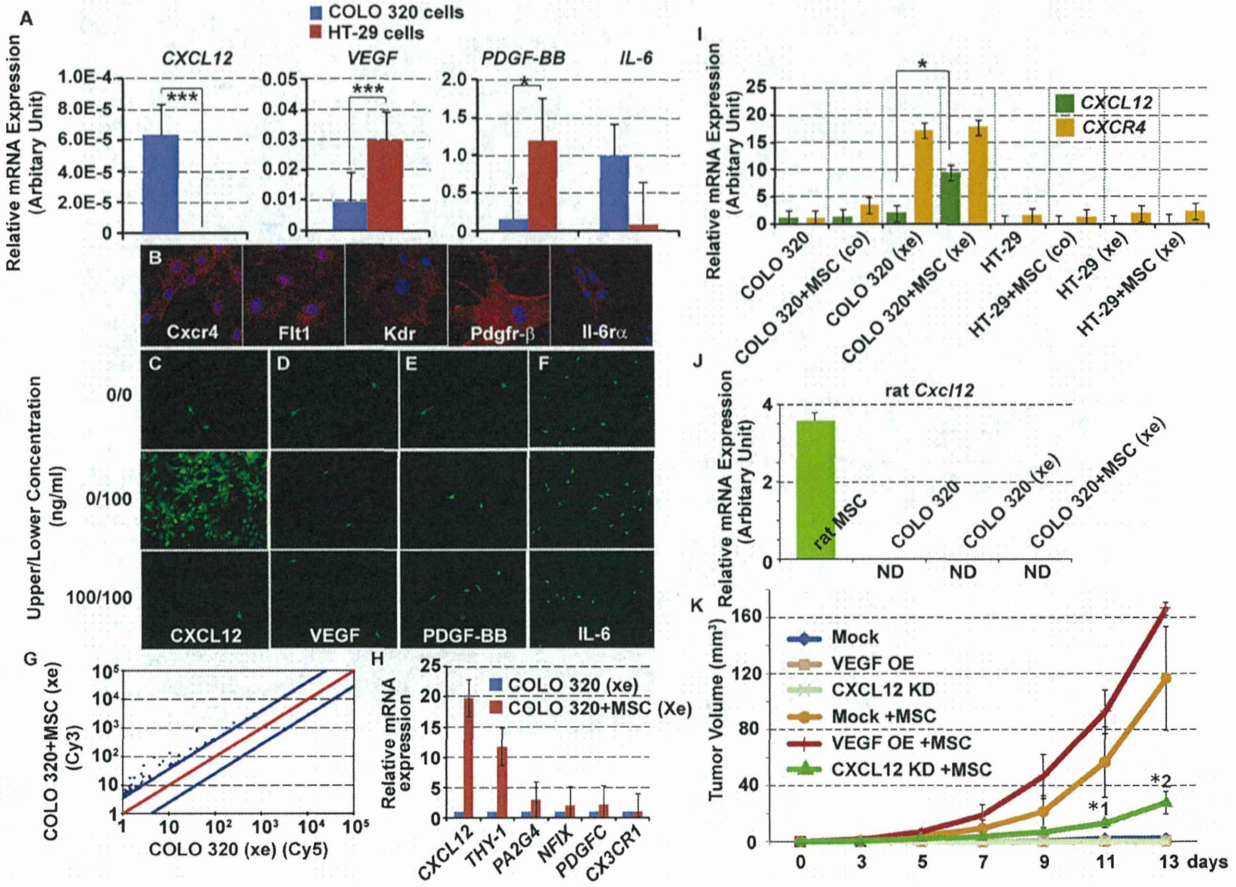


**Fig. 4** Selective activation of the CXCL12/CXCR4 axis. **a** Ligand expression was analyzed by qRT-PCR in HT-29 and COLO-320 cells. CXCL12 and IL-6 transcripts were more abundant in COLO 320 cells, whereas VEGF and PDGF-BB transcripts were significantly more abundant in HT-29 cells. **b** Expression of receptors in rat MSCs was analyzed by immunofluorescence using Alexia Fluor 594-labeled secondary antibodies. All of the corresponding receptor proteins were expressed in rat MSCs at various levels. **c–f** Chemotaxis assays were conducted with GFP-labeled MSCs seeded in upper wells and allowed to migrate toward the bottom wells containing cell-free medium with 0–100 ng/mL recombinant human chemoattractants. The assay was performed in triplicate. **g** RNA extracted from xenografts of COLO-320 cells alone or co-implanted with rat MSCs in NOG mice was analyzed using a human Oligo chip 25 K 3D-Gene (Toray) microarray. By setting the cut-off value as greater than fourfold that of the expression difference in the microarray analysis, 58 of the 25,000 genes examined were found to be more upregulated in xenografts of COLO 320 cells co-implanted with rat MSCs than in COLO 320 xenografts alone. **h** The indicated six genes among all upregulated genes were confirmed by qPCR. **i** qRT-PCR analysis of the human CXCL12/CXCR4 axis under various conditions. **j** Rat-specific Cxcl12 mRNA expression was compared in rat MSCs, COLO-320 cells, and COLO-320 xenografts with/without MSCs. **k** Growth dependency of COLO 320 cells, in which VEGF was overexpressed or CXCL12 was knocked down, on rat MSCs. Mock represented cells transduced by negative control shRNA lentivector plasmid DNA. *ND* indicates 'not detectable' and *co* and *xe* represent 'co-culture with rat MSCs' and 'xenograft tumors,' respectively. *Asterisks* indicate statistical significance. **a** $P = 6.34E{-}4$ for CXCL12, $P = 5.53E{-}5$ for VEGF, $P = 0.018$ for PDGF, **i** $P = 0.017$, and **k** *1, VEGF OE vs. CXCL12 KD $P = 0.037$, CXCL12KD vs. VEGF OE + MSC $P = 0.037$; *2, Mock vs. CXCL12 KD $P = 0.039$, VEGF OE vs. CXCL12 KD $P = 0.002$, VEGF OE vs. CXCL12 KD + MSC $P = 0.011$, CXCL12 KD vs. Mock + MSC $P = 0.039$, CXCL12 KD vs. VEGF OE + MSC $P = 0.002$, VEGF OE + MSC vs. CXCL12KD + MSC $P = 0.011$. **k** Growth dependency of COLO 320 cells, in which VEGF was overexpressed or CXCL12 was knocked down, on rat MSCs. *OE* overexpression, *KD* knock down

niche (Fig. 5b). The cytokine-producing capacity of co-cultured MSCs was analyzed by qRT-PCR (Supplementary Fig. 1f). To confirm whether CXCL12 (Fig. 4i) or Cxcl12 (Supplementary Fig. 2a) worked as a component of the cancer niche, treatment of recombinant CXCL12 (Fig. 5b) and CXCR4 antagonist (AMD3100, Fig. 5c) was included in the analyses.

## Relevant cancer cell niche signaling by MSCs

First, we chose relevant niche signaling molecules for the subsequent analyses from the candidate panel when ligands and/or receptors were upregulated in MSCs under co-cultivation with COLO 320 (Supplementary Fig. 2a). COLO 320 cell proliferation under direct contact with MSCs was

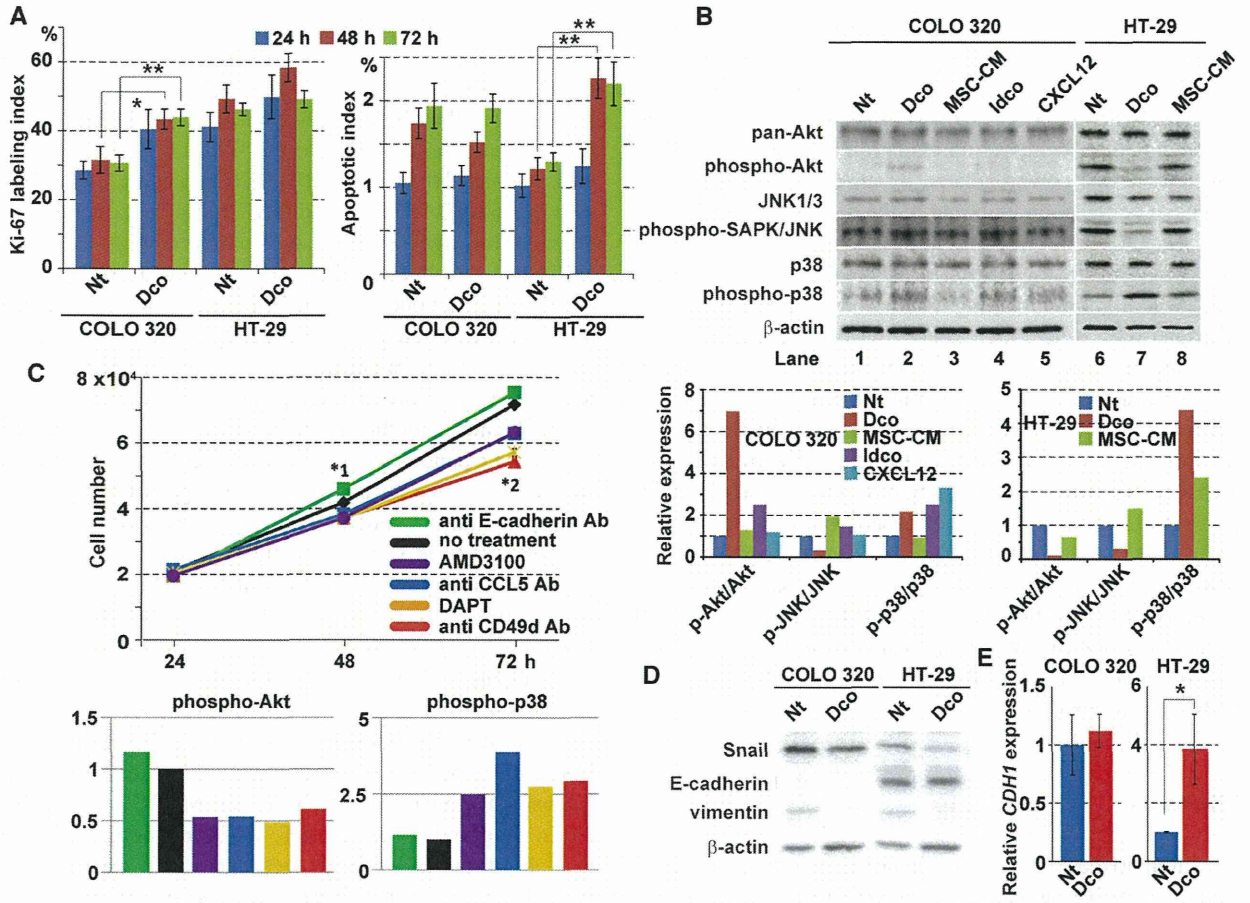


**Fig. 5** Heterotypic interactions between rat MSCs as a cancer cell niche and human colon cancer cell lines. In direct co-culture with MSCs, cancer cells were separated by FACS based on GFP fluorescence. Transwell assays were used for the indirect co-culture procedure. COLO 320 and HT-29 cells were treated with MSC-CM, and COLO 320 cells were treated with recombinant CXCL12. **a** The Ki-67 labeling index and apoptotic index calculated from TUNEL staining are shown. **b** Western blot analysis was conducted on COLO-320 and HT-29 cells cultured alone or co-cultured with MSCs and probed for the proteins shown. Data are representative of three independent experiments. Phosphorylated protein expression relative to that in untreated cells for each of the three signaling pathways was quantified in comparison to the band intensity of unphosphorylated proteins in COLO-320 (*lower left panel*) and HT-29 (*lower right panel*) cells treated as indicated. **c** Proliferation of COLO 320 cells was assessed by the cell number counted by FACS under co-culture with rat MSCs for each anti-neutralizing antibody against human E-cadherin, CCL5, and CD49d (α4 integrin), or small molecule inhibitor of the CXCL12 receptor CXCR4, AMD3100, and γ-secretase inhibitor, DAPT. Proliferation of co-cultured COLO 320 cells under no treatments was a control designated as COLO 320 (co). Phosphorylated AKT (*lower left panel*) and p38 (*lower right panel*) protein expression relative to that in untreated COLO 320 cells for each of the five signaling pathways was quantified in comparison to the band intensity in Western blot analysis (see Supplementary Fig. 2b) of unphosphorylated proteins in COLO 320 cells treated as indicated in **c**. Western blot analysis of EMT signaling molecules (**d**) and qRT-PCR analysis of *CDH1* transcripts (**e**) in direct co-culture. *Nt* no treatment, *Dco* direct co-culture, *CDH1* E-cadherin, *CXCL12* chemokine (C-X-C motif) ligand 12, *CXCR4* chemokine (C-X-C motif) receptor 4, *Ccl5* chemokine (C–C motif) ligand 5, *CCR5* chemokine (C–C motif) receptor 5, *Jag1* Jagged 1, *Vcam1* vascular cell adhesion molecule-1, *Itga4* integrin α4. *Asterisks* indicate statistical significance: co-cultured MSCs significantly increased the Ki-67 labeling index of COLO 320 cells both at 48 h ($P = 0.044$) and 72 h ($P = 0.004$), while there was an increased apoptotic index of HT-29 cells at both 48 h ($P = 0.002$) and 72 h ($P = 0.006$, **a**). **c** *1, E-cadherin vs. CD49d $P = 0.001$, E-cadherin vs. CCL5 $P = 0.002$, E-cadherin vs. DAPT $P = 4.8E{-}4$; *2, E-cadherin vs. CD49d $P = 1.0E{-}6$, E-cadherin vs. CCL5 $P = 1.1E{-}4$, E-cadherin vs. DAPT $P = 2.0E{-}6$, E-cadherin vs. AMD3100 $P = 1.3E{-}4$, control vs. CD49d $P = 3.0E{-}6$, control vs. CCL5 $P = 0.003$, control vs. DAPT $P = 2.0E{-}5$, control vs. AMD3100 $P = 0.004$, CD49d vs. CCL5 $P = 0.003$, CD49d vs. AMD3100 $P = 1.3E{-}4$. **e** $P = 0.047$

subtly enhanced by blocking homotypic E-cadherin adhesion, whereas it was suppressed by a CXCR4 antagonist (AMD3100), Ccl5 neutralization, γ-secretase inhibition (DAPT), or CD49d blockage. The major ligand of vascular cell adhesion molecule-1 (Vcam-1) is integrin α4β1 (very late antigen-4, VLA-4), which is a dimer and composed of CD49d (α4) and CD29 (β1) (Fig. 5c, Supplementary Fig. 2b). Similarly, HT-29 cell proliferation was only

enhanced by blocking E-cadherin, whereas it was suppressed by CD49d blockage. Moreover, it was not affected by CXCR4 antagonist and was not examined by Ccl5 neutralization (data not shown). Blocking E-cadherin resulted in the delicate upregulation of phospho-AKT, whereas it was downregulated by all the remaining treatments in comparison with that of the control or co-cultured COLO 320 cells without any treatments. In contrast, blocking E-cadherin did not affect the level of phospho-p38, whereas the remaining resulted in the upregulation of phospho-p38 (Fig. 5c). These results suggested that E-cadherin modestly acted as an antiproliferative signal whereas the remaining treatments functioned as growth-stimulating signals as part of the cancer niche signals in vitro. MSCs induced mesenchymal–epithelial transition (MET) along with downregulation of SNAIL and vimentin and significant upregulation of *CDH1* transcripts in HT-29 cells (Fig. 5d, e). Intriguingly, rat Cxcl12 could induce AKT signal activation as a niche signal under the heterotypic interaction between COLO 320 cells and rat MSCs (Fig. 5d, e), but recombinant human CXCL12 alone could not activate AKT (Fig. 5b) in single-cultured COLO 320 cells in vitro.

## Discussion

As summarized in Fig. 6, we demonstrated the pleiotropic action of MSCs as cancer or perivascular niche cells to modulate colorectal cancer cell fate in the xenografts. Very intriguingly, MSCs can supply contextual signals that promote COLO 320 or suppress HT-29 xenograft tumor progression. MSCs and COLO 320 cells established a functional positive feedback loop, which triggered to form a cancer cell niche through selective activation of the chemokine CXCL12/CXCR4 axis; MSCs were retained in the tumor by the CXCL12/Cxcr4 axis, in turn, retained MSCs enhanced AKT signals in COLO 320 cells potentially through Cxcl12/CXCR4 in concert with other niche signals, such as Vcam-1/VLA-4, Jagged1/NOTCH-4, Ccl5/chemokine (C–C motif) receptor 5 (CCR5) as Karnoub et al. [6] previously reported under direct cell–cell contact. Subsequently, MSCs differentiated into pericytes enhanced angiogenesis as a perivascular niche in which mouse angiogenic cells properly differentiated into endothelial cells to form tumor vessels (Fig. 3). In contrast to COLO 320, MSCs as the cancer cell niche exerted an anti-proliferative property to HT-29 cells potentially through MET signaling resulting in activation of p38 in vitro. As depicted in the dashed line in Fig. 6, an anti-proliferative signal from MSCs were so modest that it could be overwhelmed by vigorous proliferation of HT-29 in vivo, leading to spurious MSC-independency. However, what grants MSCs such a context-dependent niche cell function has been the central question of niche biology. Khakoo et al. [5] reported that MSCs exert potent antitumorigenic effects in a model of Kaposi's sarcoma. They showed that MSCs could inhibit the in vitro activation of AKT, which requires the MSCs to make direct cell–cell contact, and which could be inhibited by blocking E-cadherin. Very recently, we demonstrated that MSCs canceled azoxymethane-induced tumor initiation [30]. These results appeared to be along antitumor Khakoo's line of view.

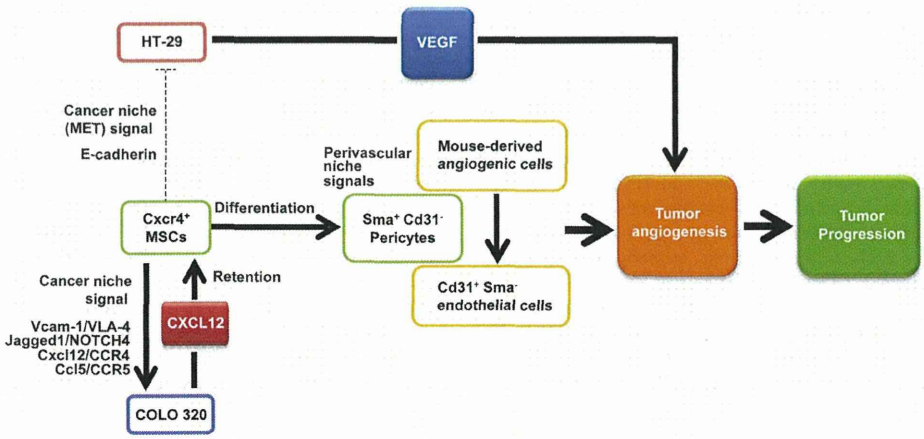


**Fig. 6** Schema of tumor modulation by MSCs as niche cells. Although HT-29 xenografts sustain negative MET signals from a MSC niche, overwhelmingly progress through VEGF-mediated active tumor angiogenesis. In contrast, COLO 320 xenografts cannot progress unaided by coordinating cancer niche signals composed of Vcam-1/VLA-4, Jagged1/NOTCH4, Cxcl12/CCR4, and Ccl5/CCR5 because they scarcely produced VEGF. COLO 320 cells retained MSCs via chemotactic interaction and promoted by the cancer niche signals. Furthermore, MSCs provide perivascular niche signals to promote so-called 'MSC-dependent angiogenesis'

Xenograft analyses suggest that colon cancer cell lines fall into two categories: MSC-independent cell lines such as HT-29 and MSC-dependent cell lines such as COLO 320. The host tumor immune surveillance is known to dominantly affect tumor engraftment [4] even though xenograft rejection in these immunodeficient mice must be further attenuated by the immunosuppressive property of co-implanted MSCs or, in contrast, must be further enhanced by eGFP immunogenicity derived from co-implanted MSCs. In either case, host immune competency cannot explain the cell line-specific growth dependency on MSCs, but can seriously affect tumor engraftment. To determine why the cell lines were MSC-dependent, we established stable CXCL12 KD or VEGF OE COLO 320 cells (Fig. 4k). CXCL12 KD cells significantly suppressed tumor growth. Although VEGF OE cells significantly enhanced tumor growth, co-implantation of MSCs was still necessary, namely, they remain MSC-dependent. The mechanism determining MSC dependency is still an open question. Collectively, we hypothesize that the MSC-dependency may be evidence of the niche function of MSCs, because MSCs try to inhibit vigorously proliferating stem cells while supporting dormant stem cells, analogous to maintaining the milieu of the stem cell niche and leading to MSC-dependency of partner cells. Further studies are necessary to test this attractive hypothesis.

In vitro co-culture experiments showed that MSCs enhanced AKT signals in COLO 320 cells potentially through Cxcl12/CXCR4, Ccl5/CCR5, Vcam1/VLA-4, and Jagged1/Notch4 interaction in a coordinated manner (Fig. 5). Among them, Cxcl12 could induce AKT signal activation as a niche signal under the heterotypic interaction between COLO 320 cells and MSCs (Fig. 5d, e) but recombinant CXCL12 could not activate AKT in single-cultured COLO 320 cells (Fig. 5b). In contrast to the above in vitro findings, human *CXCL12* transcripts could be significantly induced by MSCs in co-implanted xenograft tumors by an unknown mechanism (Fig. 4i), whereas rat Cxcl12 transcripts were so rare that they could not be detected by qRT-PCR in the co-implanted xenograft tumors (Fig. 4j). These suggest that the paracrine interspecific Cxcl12/CXCR4 axis appears to be more relevant as a niche signal in vivo than the autocrine human CXCL12/CXCR4 axis. Both CXCL12 and CXCR4 were expressed in COLO 320 cells, while both were also expressed in MSCs. Among these, CXCL12/Cxcr4 was used for chemotactic retention of MSCs in the tumor (Fig. 4c), whereas Cxcl12/CXCR4 was likely used for the growth-stimulating signal in vitro co-culture of COLO 320 cells with MSCs. Augmentation of the CXCL12/CXCR4 axis in xenografts with co-implanted MSCs (Fig. 4g, i) suggested that a functional positive feedback loop was triggered through the above series of interactions forming a niche between MSCs and COLO 320 cells in vivo.

There remain many unresolved issues related to this area of research in the current study. First, we based our study on a somewhat complicated xenograft model involving cross-species interactions among human colorectal cancer cells, rat MSCs, and host mouse cells. It is noteworthy that our results can only reflect effects mediated by those molecules which may be cross-reactive across the species involved. For example, although IL-6 [29] as well as VEGF [31] are known attractants for MSCs, chemotaxis was not observed in this study. It is likely because a ligand/receptor of IL-6 and VEGF axis are less homologous between human and rat than that of CXCL12 axis. Therefore, our results cannot be extrapolated directly to human tumorigenesis. A validation study should be conducted using human MSCs. Second, MSCs as a cancer niche stimulate tumor growth of COLO 320 cells, but suppress tumor growth of HT-29 cells. For such growth stimulation, further studies are required to clarify the in vivo mechanisms inducing selective activation of CXCL12 (Fig. 4i) as depicted in Supplementary Fig. 2c–e. For growth-inhibition via MET (Fig. 5f), although we demonstrated that MSCs induce MET signals in human colorectal cancer cells, there is a conflicting report showing that MSCs induce EMT through the expression of surface-bound transforming growth factor-β (TGF-β) [16]. Further studies are necessity to resolve the enigma of emerging contextual signals from the MSC niche. Next, cell origin and tumor topography of recruited mouse angiogenic cells remain to be clarified, including whether they were endothelial progenitor cells (EPC) [32] or adequately recruited into neoangiogenic fields. Finally, MSCs can engraft and function as at least two types of niches: one for CAFs as the cancer cell niche to modulate tumor progression, and the other for pericytes as the perivascular niche in MSC-dependent angiogenesis. It should be confirmed which niches are essential for MSC dependency on tumor progression. To this end, other cell lines should undergo further detailed analyses.

We conclude that MSCs that form a cancer cell niche can supply contextual signals towards colorectal tumor growth. These results introduce some reservations about the broader clinical applications of seemingly promising MSC-based therapies. Before proceeding, we should further clarify the potential risks or benefits of such therapies on colorectal tumor progression. Further exploration of the functions of MSCs as a cancer cell niche is warranted to provide alternative therapeutic options for colorectal cancer.

**Acknowledgments** We are very grateful to Ms. K. Fujii of First Department of Internal Medicine, for technical assistance, and Dr. Y. Sasaki of Medical Genome Sciences, Research Institute for

Frontier Medicine, Sapporo Medical University, for critical comments. We are also thankful to Dr. M. Tsuji of Chromosome Science Labo Inc., for providing FISH probes and technical advice. This work was supported in part by Health and Labor Sciences Research Grants for research on intractable diseases from the Ministry of Health, Labour, and Welfare of Japan (K.I. and Y.A.).

**Conflict of interest** The authors declare that they have no conflict of interest.

## References

1. Bissell MJ, Radisky D. Putting tumours in context. Nat Rev Cancer. 2001;1:46–54.
2. Hall B, Andreeff M, Marini F. The participation of mesenchymal stem cells in tumor stroma formation and their application as targeted-gene delivery vehicles. Handb Exp Pharmacol. 2007;263–83.
3. Park CC, Bissell MJ, Barcellos-Hoff MH. The influence of the microenvironment on the malignant phenotype. Mol Med Today. 2000;6:324–9.
4. Hanahan D, Weinberg RA. Hallmarks of cancer: the next generation. Cell. 2011;144:646–74.
5. Khakoo AY, Pati S, Anderson SA, et al. Human mesenchymal stem cells exert potent antitumorigenic effects in a model of Kaposi's sarcoma. J Exp Med. 2006;203:1235–47.
6. Karnoub AE, Dash AB, Vo AP, et al. Mesenchymal stem cells within tumour stroma promote breast cancer metastasis. Nature. 2007;449:557–63.
7. Tanaka H, Arimura Y, Yabana T, et al. Myogenic lineage differentiated mesenchymal stem cells enhance recovery from dextran sulfate sodium-induced colitis in the rat. J Gastroenterol. 2011;46:143–52.
8. Yabana T, Arimura Y, Tanaka H, et al. Enhancing epithelial engraftment of rat mesenchymal stem cells restores epithelial barrier integrity. J Pathol. 2009;218:350–9.
9. Hogan NM, Dwyer RM, Joyce MR, Kerin MJ. Mesenchymal stem cells in the colorectal tumor microenvironment: recent progress and implications. Int J Cancer. 2012;131:1–7.
10. Tsai K-S, Yang S-H, Lei Y-P, et al. Mesenchymal stem cells promote formation of colorectal tumors in mice. Gastroenterology. 2011;141:1046–56.
11. Shinagawa K, Kitadai Y, Tanaka M, et al. Mesenchymal stem cells enhance growth and metastasis of colon cancer. Int J Cancer. 2010;127:2323–33.
12. De Boeck A, Pauwels P, Hensen K, et al. Bone marrow-derived mesenchymal stem cells promote colorectal cancer progression through paracrine neuregulin 1/HER3 signalling. Gut. 2013;62:550–60.
13. Lin J-T, Wang J-Y, Chen M-K, et al. Colon cancer mesenchymal stem cells modulate the tumorigenicity of colon cancer through interleukin 6. Exp Cell Res. 2013;319:2216–29.
14. Liu Y, Han Z, Zhang S, et al. Effects of inflammatory factors on mesenchymal stem cells and their role in the promotion of tumor angiogenesis in colon cancer. J Biol Chem. 2011;286:25007–15.
15. Li H-J, Reinhardt F, Herschman HR, Weinberg RA. Cancer-stimulated mesenchymal stem cells create a carcinoma stem cell niche via prostaglandin E2 signaling. Cancer Discov. 2012;2:840–55.
16. Mele V, Muraro MG, Calabrese D, et al. Mesenchymal stromal cells induce epithelial-to-mesenchymal transition in human colorectal cancer cells through the expression of surface-bound TGF-β. Int J Cancer. 2014;134:2583–94.
17. Hakamata Y, Tahara K, Uchida H, et al. Green fluorescent protein-transgenic rat: a tool for organ transplantation research. Biochem Biophys Res Commun. 2001;286:779–85.
18. Ito M, Hiramatsu H, Kobayashi K, et al. NOD/SCID/gamma(c)(null) mouse: an excellent recipient mouse model for engraftment of human cells. Blood. 2002;100:3175–82.
19. Dominici M, Le Blanc K, Mueller I, et al. Minimal criteria for defining multipotent mesenchymal stromal cells. The International Society for Cellular Therapy position statement. Cytotherapy. 2006;8:315–7.
20. Javazon EH, Colter DC, Schwarz EJ, Prockop DJ. Rat marrow stromal cells are more sensitive to plating density and expand more rapidly from single-cell-derived colonies than human marrow stromal cells. Stem Cells. 2001;19:219–25.
21. Kuan SF, Byrd JC, Basbaum CB, Kim YS. Characterization of quantitative mucin variants from a human colon cancer cell line. Cancer Res. 1987;47:5715–24.
22. Livak KJ, Schmittgen TD. Analysis of relative gene expression data using real-time quantitative PCR and the 2(−Delta Delta C(T)) method. Methods. 2001;25:402–8.
23. Weidner N, Semple JP, Welch WR, Folkman J. Tumor angiogenesis and metastasis—correlation in invasive breast carcinoma. N Engl J Med. 1991;324:1–8.
24. Iyonaga K, Takeya M, Yamamoto T, et al. A novel monoclonal antibody, RM-4, specifically recognizes rat macrophages and dendritic cells in formalin-fixed, paraffin-embedded tissues. Histochem J. 1997;29:105–16.
25. Tamaki T, Akatsuka A, Okada Y, et al. Cardiomyocyte formation by skeletal muscle-derived multi-myogenic stem cells after transplantation into infarcted myocardium. PLoS ONE. 2008;3:e1789.
26. Grunewald M, Avraham I, Dor Y, et al. VEGF-induced adult neovascularization: recruitment, retention, and role of accessory cells. Cell. 2006;124:175–89.
27. Wynn RF, Hart CA, Corradi-Perini C, et al. A small proportion of mesenchymal stem cells strongly expresses functionally active CXCR4 receptor capable of promoting migration to bone marrow. Blood. 2004;104:2643–5.
28. Karp JM, Leng Teo GS. Mesenchymal stem cell homing: the devil is in the details. Cell Stem Cell. 2009;4:206–16.
29. Rattigan Y, Hsu J-M, Mishra PJ, et al. Interleukin 6 mediated recruitment of mesenchymal stem cells to the hypoxic tumor milieu. Exp Cell Res. 2010;316:3417–24.
30. Nasuno M, Arimura Y, Nagaishi K, et al. Mesenchymal stem cells cancel azoxymethane-induced tumor initiation. Stem Cells. 2014;32:913–25.
31. Vertelov G, Kharazi L, Muralidhar MG, et al. High targeted migration of human mesenchymal stem cells grown in hypoxia is associated with enhanced activation of RhoA. Stem Cell Res Ther. 2013;4:5.
32. Orimo A, Gupta PB, Sgroi DC, Arenzana-Seisdedos F, Delaunay T, Naeem R, et al. Stromal fibroblasts present in invasive human breast carcinomas promote tumor growth and angiogenesis through elevated SDF-1/CXCL12 secretion. Cell. 2005;121:335–48.